JOURNAL OF PROTEOMICS 79 (2013) 180–194

Available online at www.sciencedirect.com

SciVerse ScienceDirect

www.elsevier.com/locate/jprot

Application of integrated transcriptomic, proteomic and metabolomic profiling for the delineation of mechanisms of drug induced cell stress

Anja Wilmes[a,1], Alice Limonciel[a,1], Lydia Aschauer[a,1], Konrad Moenks[b,1], Chris Bielow[c], Martin O. Leonard[d], Jeremy Hamon[e,f], Donatella Carpi[g], Silke Ruzek[h], Andreas Handler[h], Olga Schmal[i], Karin Herrgen[i], Patricia Bellwon[i], Christof Burek[i], Germaine L. Truisi[j,m], Philip Hewitt[j], Emma Di Consiglio[k], Emanuela Testai[k], Bas J. Blaauboer[l], Claude Guillou[g], Christian G. Huber[h], Arno Lukas[b], Walter Pfaller[a], Stefan O. Mueller[j,m], Frederic Y. Bois[e,f], Wolfgang Dekant[i], Paul Jennings[a,*,1]

[a]Division of Physiology, Department of Physiology and Medical Physics, Innsbruck Medical University, Innsbruck 6020, Austria
[b]Emergentec Biodevelopment GmbH, Vienna 1180, Austria
[c]Institute of Computer Science, Department of Mathematics and Computer Science, Freie Universität Berlin, Berlin 14195, Germany
[d]University College Dublin, School of Medicine and Medical Science, Conway Institute of Biomolecular and Biomedical Research, Dublin D4, Ireland
[e]INERIS, DRC/VIVA/METO, France
[f]Université de Technologie de Compiègne, Compiègne Cedex, 60205, France
[g]European Commission, Joint Research Centre, Institute for Health and Consumer Protection, Systems Toxicology Unit, Ispra (VA) 21027, Italy
[h]Department of Molecular Biology, Division of Chemistry and Bioanalytics, University of Salzburg, Salzburg 5020, Austria
[i]Department of Toxicology, University of Würzburg, Würzburg 97078, Germany
[j]Merck KGaA, Merck Serono, Nonclinical Safety, Darmstadt 64293, Germany
[k]Environment and Primary Prevention Department, Istituto Superiore di Sanità, Rome 00161, Italy
[l]Institute for Risk Assessment Sciences, Utrecht University, Utrecht 3508, The Netherlands
[m]Institut für Angewandte Biowissenschaften, Karlsruhe Institute of Technology (KIT), Karlsruhe 76131, Germany

ARTICLE INFO

Article history:
Received 6 September 2012
Accepted 24 November 2012
Available online 10 December 2012

Keywords:
Cyclosporine A
Integrated omics
ATF4
Nrf2
Unfolded protein response
Cyclophilin

ABSTRACT

High content omic techniques in combination with stable human *in vitro* cell culture systems have the potential to improve on current pre-clinical safety regimes by providing detailed mechanistic information of altered cellular processes. Here we investigated the added benefit of integrating transcriptomics, proteomics and metabolomics together with pharmacokinetics for drug testing regimes.

Cultured human renal epithelial cells (RPTEC/TERT1) were exposed to the nephrotoxin Cyclosporine A (CsA) at therapeutic and supratherapeutic concentrations for 14 days. CsA was quantified in supernatants and cellular lysates by LC–MS/MS for kinetic modeling. There was a rapid cellular uptake and accumulation of CsA, with a non-linear relationship between intracellular and applied concentrations. CsA at 15 μM induced mitochondrial disturbances and activation of the Nrf2-oxidative-damage and the unfolded protein-response pathways. All three omic streams provided

* *Corresponding author at*: Division of Physiology, Department of Physiology and Medical Physics, Innsbruck Medical University, Fritz-Pregl Strasse 3, 6020, Innsbruck, Austria.
E-mail addresses: paul.jennings@i-med.ac.at, paul.other@gmail.com (P. Jennings).
[1] Equal contributing authors.

http://dx.doi.org/10.1016/j.jprot.2012.11.022

complementary information, especially pertaining to Nrf2 and ATF4 activation. No stress induction was detected with 5 μM CsA; however, both concentrations resulted in a maximal secretion of cyclophilin B.
The study demonstrates for the first time that CsA-induced stress is not directly linked to its primary pharmacology. In addition we demonstrate the power of integrated omics for the elucidation of signaling cascades brought about by compound induced cell stress.

1. Introduction

Failures of lead candidates in the late phases of pharmaceutical development are costly, both in terms of time and money and thus seriously hinder the number of compounds reaching the market. Compounds are dropped late in development, due to a lack of efficacy or to unexpected adverse effects that were not identified by animal test batteries. The EU 7th Framework project, Predict-IV, was established in order to develop mechanistic strategies for predictive toxicology. We are pursuing three avenues simultaneously in an attempt to improve pre-clinical safety test systems by: (i) focusing on cells of human origin, (ii) conducting in-depth characterization of molecular perturbations with complimentary omic technologies and (iii) determining the actual compound exposure through pharmacokinetic modeling.

Developments in cell culture techniques such as the availability of hormonally defined media together with recent advances in immortalization including stable expression of the catalytic subunit of human telomerase have led to the generation of improved cell lines such as the human renal proximal tubular cell line, RPTEC/TERT1 [1]. However, cell cultures have not yet reached their full potential as a tool for toxicological investigations, as they have been mostly used in conjunction with cytotoxicity end-points providing little mechanistic information. Molecular analysis of cellular processes in response to compound exposure would better harness the potential of *in vitro* systems. Recent technological advancements allow the possibility of a holistic, mechanistic approach to *in vitro* toxicology and promise to further our understanding of how cells deal with stress.

Omic-profiling-techniques have proven to be powerful new tools for unraveling complex biological processes and have been successfully utilized in the fields of microbiology, fungal, plant and human biology [2–5]. Transcriptomic (TCX) studies cover the entire human genome and are well established. TCX has been used in many *in vitro* and *in vivo* studies [6–9]. However, gene expression alone does not provide information on alternative splicing, PTM or even protein expression itself. Proteomics (PTX) offers the possibility to directly study the expressed protein, including isoforms and PTMs. However, it is not yet possible to study the entire proteome and factors such as protein abundance level, p*I* and solubility, come into play. Thus the number of proteins detected is dependent on the protocols employed for isolation, enrichment and separation. Metabolomics (MTX) provides a snapshot of the metabolic environment that is the consequence of the transcriptome, proteome and nutritional environment. Both PTX and MTX are now beginning to be utilized in toxicological and pharmacological settings [10,11]. The integration of these three omic technologies has the potential to give a much more detailed view of cellular homeostasis than when used individually [12]. In addition, for a correct interpretation of toxicological data, it is critical to have information on the cellular handling of the applied compound. This can be approached using pharmacokinetic modeling [13].

The major aim of this study was to investigate the benefit of integrating omic data streams with pharmacokinetics for use in *in vitro* toxicology and safety assessment. We show, under our experimental settings, that this approach provided a global picture of compound-induced stress and could clearly distinguish pharmacological from toxicological effects.

2. Materials and methods

Chemicals were purchased from Sigma Aldrich, unless otherwise stated.

2.1. Cell culture

RPTEC/TERT1 [1] cells were obtained from Evercyte GmbH, Vienna and cultured in a 1 to 1 mixture of DMEM and Ham's F-12 nutrient mix (Invitrogen) supplemented with 2 mM glutamax (Invitrogen), 5 μg/ml insulin, 5 μg/ml transferrin and 5 ng/ml sodium selenite, 100 U/ml penicillin and 100 μg/ml streptomycin, 10 ng/ml epithelial growth factor and 36 ng/ml hydrocortisone.

2.2. Cell treatment and sample preparation

RPTEC/TERT1 cells were cultured on 0.2 μm pore size, 25 mm diameter aluminum oxide filters (Nunc), with 1 ml apical and 2 ml basolateral medium. CsA (Calbiochem, purity 97%) was dissolved in DMSO and further diluted in culture medium to 5 and 15 μM. DMSO concentration was 0.1% in both CsA medium and control medium. After a 10 day stabilization phase, cells were treated with CsA every day for up to 14 days. Cells were harvested at days 1, 3 and 14 for TCX, PTX, and MTX (Fig. 1a). Additionally, supernatant was collected daily for MTX and CsA was measured in supernatants, cell lysates and on cell culture walls (Fig. 1a). RNA was extracted using the RNeasy Mini Kit (QIAGEN). For PTX, MTX and kinetics ice cold 100% methanol was used as a quenching and lysing reagent. For MS MTX cells were washed in ammonia bicarbonate (185 mM, pH 7.8) prior to lysing. CsA bound to cell culture wells was removed with 100% methanol.

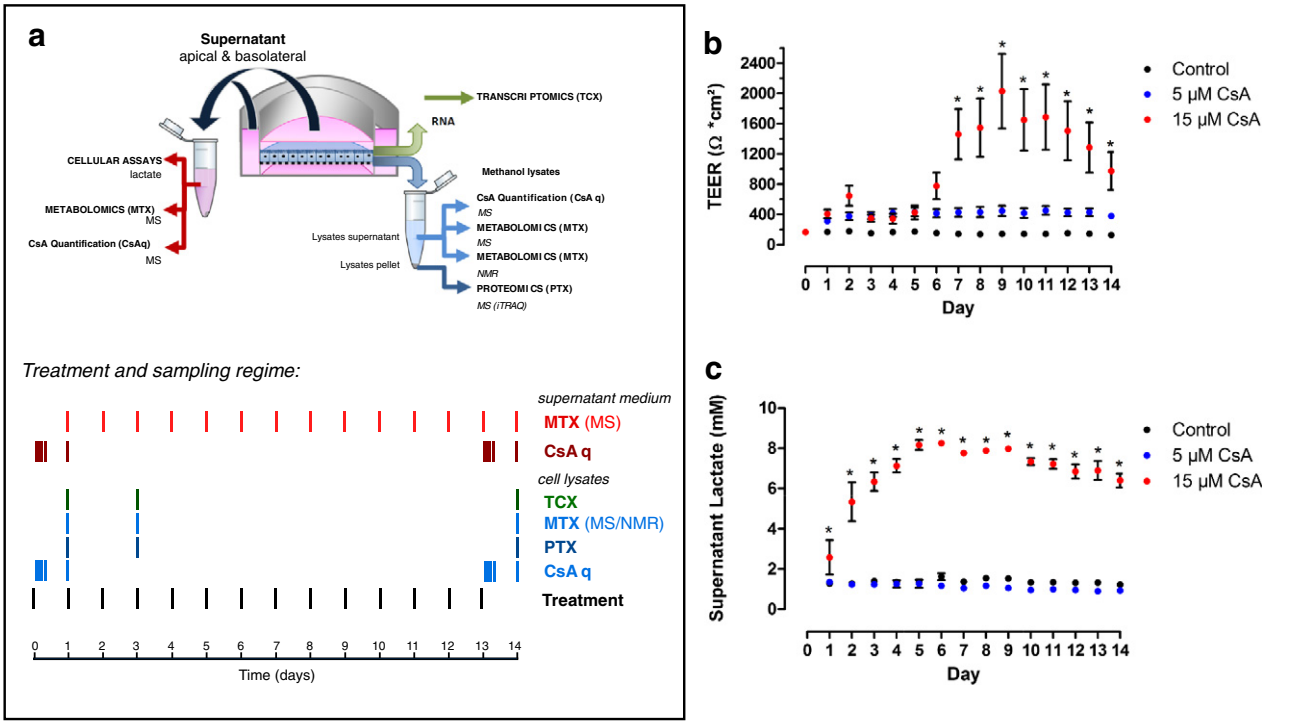

Fig. 1 – Experimental layout and effects of treatment on monitoring endpoints. (a) Scheme of experimental procedure and sample generation. RPTEC/TERT1 cells, cultured on microporous supports, were stabilized for 10 days and treated with CsA. Samples were harvested at set intervals as indicated. Transepithelial electrical resistance (TEER) (b) and lactate (c) were measured daily. Values represent the mean ± SEM of three biological replicates. *Denotes a significant difference (0.05) from controls using repeated measures two-way ANOVA with a Bonferroni's multiple comparisons post test.

2.3. *Monitoring endpoints*

Transepithelial electrical resistance (TEER) was measured using the Endohm and EVOM systems from World Precision Instruments. Supernatant lactate was quantified using a biochemical assay [14]. Statistical analysis was performed using a two-way ANOVA with a Bonferroni's multiple comparisons post test (n = 3).

2.4. *Omic and CsA quantification procedures*

TCX was conducted with Illumina® HT 12 v3 BeadChip arrays (~47,000 transcripts). Peptides for PTX were labeled with iTRAQ and measured with HPLC-MS. The HPLC system was directly coupled to a linear ion-trap Orbitrap mass spectrometer (LTQ Orbitrap XL, ThermoFisher Scientific) with a nanoelectrospray ionization source operated in positive ionization mode. MS MTX profiling of cell lysates was also conducted with Orbitrap MS with direct infusion. ^{1}H NMR spectra from cell lysates were recorded at 600.13 MHz on a Bruker DMX 600 Spectrometer equipped with a 5 mm DCH cryoprobe at 303 K. Supernatant medium was analyzed by LC–MS, where separation was performed on an Ultimate 3000 liquid chromatography system (Dionex) followed by on-line analysis with an Orbitrap mass spectrometer. CsA was quantified by LC–MS/MS using a calibration curve with a linear range between 10 nM and 2000 nM.

Detailed procedures are given in the Supplementary Methods.

2.5. *Western blot analysis*

For cyclophilin B blots, methanol extracts were evaporated and resuspended in 30 mM Tris–HCl, 7 M urea, 2 M thiourea and 4% (w/v) CHAPS, pH 8.5. Cell lysates (5 µg) and supernatants (16 µl) were loaded. In order to study the nuclear and the cytosolic fraction RPTEC/TERT1 cells cultured in 12 well plates were treated every day for up to 14 days with 5 and 15 µM CsA and with 5 µM of the Nrf2 activator AI1. Cells were lysed and nuclear and cytosolic fractions were prepared as previously described [6]. Samples (10 to 20 µg) were separated on a 4–12% gradient Nu-Page Bis-Tris SDS-PAGE gel and transferred to PVDF membranes. Antibody sources and dilutions are given in the Supplementary Methods.

2.6. *Data warehousing, data analysis and statistics*

Collection and warehousing of omic data were performed using BASE (Emergentec Biodevelopment GmbH, www.emergentec.com). Identification of deregulated TCX probes was carried out using a moderated one-way ANOVA to reduce the set of relevant probes to those that exhibit a significant change under any condition with a Benjamini–Hochberg corrected p-value below or equal to 0.05. On the remaining probes, a moderated two-sided *t*-test was calculated and corrected *via* Benjamini–Hochberg. For both steps, the R package "limma" was used. Pathway and transcription factor

enrichment was conducted with Ingenuity Pathway Analysis (IPA®, www.ingenuity.com/), using a fold cutoff of 1.5 and p-value of 0.001. Heat maps were generated with Treeview (rana.lbl.gov/EisenSoftware). Principal component analysis (PCA) plots were generated using prcomp in the R package "stats".

Protein identification and quantification workflow were implemented in OpenMS (version 1.9) [15] and TOPPAS [16]. Statistical analysis was performed using the isobar package [17] and custom R code. For additional details see the Supplementary Methods.

The software package BRB-ArrayTools was used to identify significantly altered features in the supernatant MTX data [18]. A class comparison with less than 0.001 p-value and 2 fold alteration from treated to time matched control was used.

2.7. *Pharmacokinetic analysis*

To analyze the *in vitro* pharmacokinetic CsA data, we developed a 3-compartment model of CsA exchange between supernatant, cells and vial wall (Fig. 5a). CsA could distribute inside the cells, attach to the plastic vial walls and be metabolized. Several mathematical forms for exchange rates were tested: the best fit was obtained using a first order entry into cells with Michaelis–Menten (saturable) exit rate, a first order attachment to vial wall with non-integer (fractal) order detachment, and Michaelis–Menten metabolism. For further details see the Supplementary Methods.

3. Results

We aimed to investigate the effects of repeated exposure of Cyclosporine A (CsA) at concentrations where no major cellular perturbations are observed (upper therapeutic index) and where severe perturbations are observed, but in the absence of cell death. Previous experiences demonstrated that a 14 day repeated dose regime of 5 and 15 μM would fit these criteria [14]. TEER and lactate production were monitored through-out the experiment as parameters of monolayer integrity and cell stress, respectively [14,19]. We observed an early increase in TEER with 15 μM CsA that was significantly elevated at day 7 and this elevation was maintained until day 14 (Fig. 1b). Such an effect has been previously documented [20] and is thought to be due to alterations in claudin expression. In our TCX data, we have also observed such changes. There was no significant impact of 5 μM CsA on TEER over the 14 days. Lactate production was unaltered by 5 μM CsA but was significantly elevated by 15 μM CsA, starting at day 1 (Fig. 1c). Thus, two independent parameters demonstrated a major perturbation of cellular function with 15 μM CsA in the absence of significant toxicity.

3.1. *TCX alterations*

Apart from one gene (the chloride channel, *CLCNKA*, d1 vs d14), there were no time-dependent alterations in the control samples. This illustrates the stability of the model over the treatment period. CsA at 5 μM had no significant impact on the transcriptome. For 15 μM CsA, there were 3314, 3968 and 1337 probes differently expressed at 1, 3 and 14 days, respectively. PCA confirmed these observations (Fig. 2a). The highest transcriptomic impact was observed after 3 days, while 14 days had the least impact. Pathway analysis, using IPA® identified protein ubiquitination, Nrf2-mediated-oxidative-stress response, glutathione metabolism and aminoacyl-tRNA biosynthesis as major hubs (Fig. 2b). Transcription factor enrichment analysis showed a predominance of Nrf2, XBP1 and ATF4 activation at all time points (Fig. 2c). Individual gene changes from these pathways are depicted in Fig. 2d as heat maps.

There was a clear activation of all three branches of the *unfolded protein response* (UPR) with 15 μM CsA. Genes that have been well characterized from the PERK/ATF4 branch include those involved in amino acid synthesis, amino acid transport (including *SLC7A5* and *11*) and aminoacyl-tRNA synthesis (Fig. 2d). There was also a clear activation of the UPR-ATF6-branch with induction of *HSPA5*, *XBP1 HSP90B1*, *DDIT3* and *WFS1*. The UPR IRE1 branch/XBP1 was also activated, including induction of *SERP-1*, and the DnaJ (Hsp40) homologs *DNAJB11* and *DNAJB9*.

Nrf2-oxidative-stress-pathway was induced by 15 μM CsA. Nrf2-dependent genes induced at all time points include genes involved in glutathione synthesis (*GCLM* and *GCLC*), glutathione recycling (*GSR*), genes with an anti-oxidant role (*SRXN1*, *TXN*, *TXNRD1*, *SOD1*) and iron storage (*FTH1*) (Fig. 2d). *NQO1* and heme oxygenase 1 (*HMOX1*, aka *HO1*) were induced at the early time points. Additionally, *ATF4* mRNA, which is under the transcriptional regulation of Nrf2 [21] was increased.

CsA caused a robust alteration in genes involved in protein degradation (Fig. 2d). These include those involved in (i) chaperone activity (DnaJ (Hsp40) homologs and heat shock protein (HSP) family), (ii) ubiquitination (ubiquitin-conjugating enzymes (UBE) and ubiquitin specific peptidases (USP)), (iii) proteasome activity (proteasome (prosome, macropain) subunits (PSM)) and (iv) lysosomal activity (*PSAP* and *CTSD*).

CsA (15 μM) also resulted in an alteration of genes involved in *glycolysis* and the *p53 pathway*. These included the induction of hexokinase 2 (*HK2*), enolase 2 (*ENO2*), *CDKN1A* (aka p21) and growth arrest and DNA-damage-inducible, alpha (*GADD45A*).

Members of the peptidylprolyl isomerase family (PPI), better known as cyclophilins (CyP), were also altered in the TCX data by 15 μM CsA (Fig. 2d). The cytosolic isoform *CyP-C* (aka *PPIC*) was decreased on all days. The mitochondrial *CyP-D* (encoded by *PPIF*) and *CyP-G* (aka *PPIG*) were increased at day 3 and *CyP-H* (aka *PPIH*) was decreased at day 1.

3.2. *PTX alterations induced by CsA*

A total of 218 out of 2642 proteins detected, of which 599 were detected in every condition, were significantly altered by 15 μM CsA. PCA shows a strong separation of both concentrations (Fig. 3a). The fold expression levels of 15 μM CsA-altered proteins were correlated to their respective mRNA values at each time point (Fig. 3b). Day 1 had the poorest correlation that improved considerably with time. However, for certain proteins there was no correlation or an inverse correlation to the

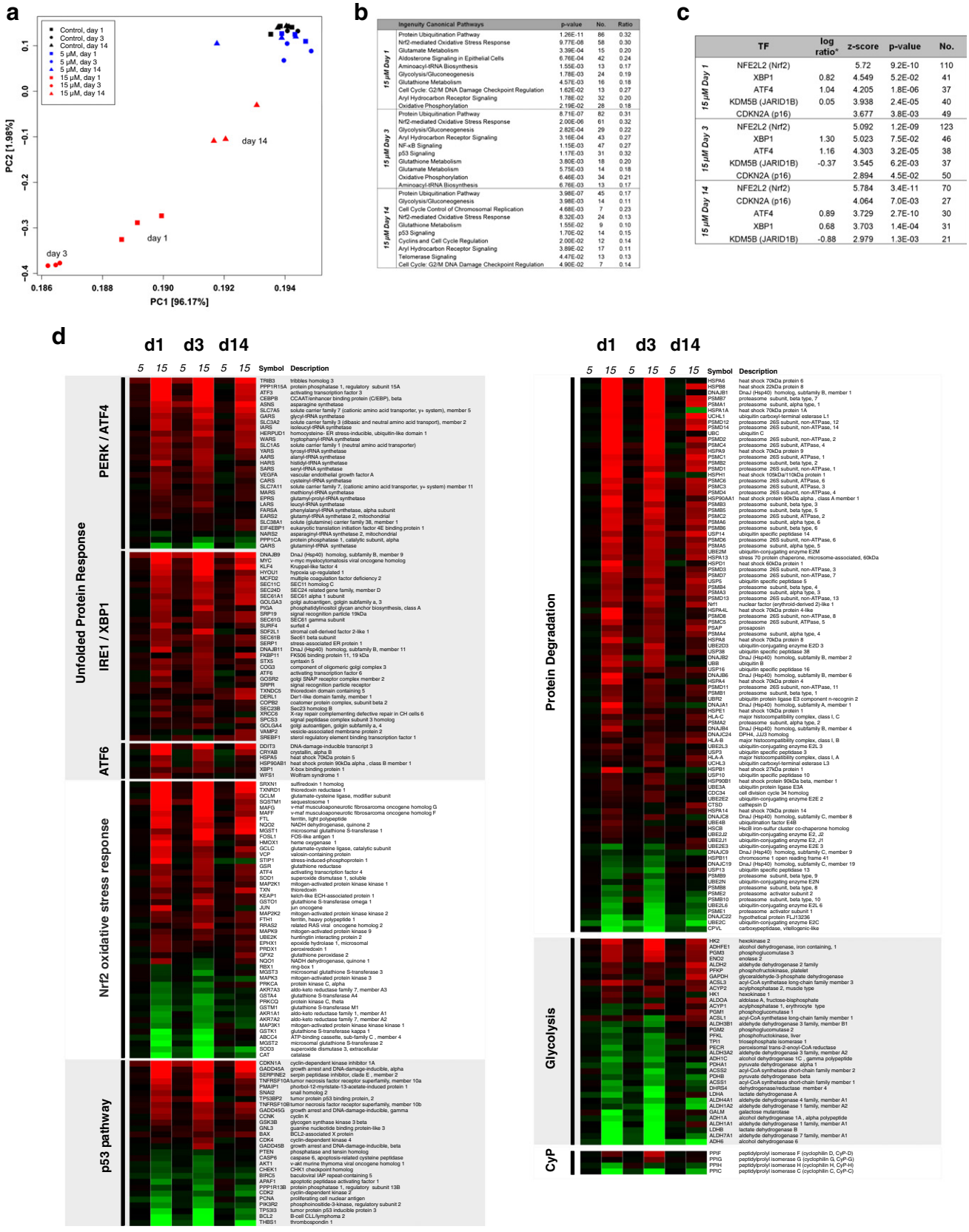

Fig. 2 – Effects of CsA exposure on RPTEC/TERT1 transcriptome. (a) Principal component analysis (PCA) of all probes from the 27 arrays. (b) IPA® summary of enriched canonical pathways. The ratio is the number of identified molecules divided by the number of molecules in the pathway. (c) IPA® prediction of transcription factor (TF) involvement. The p-value is calculated with Fisher's exact test. The z-score predicts TF state, where z>2 is significantly activated. * Log ratio is given where the transcript itself was deregulated. (d) The actual values (log 2 fold control) are shown as a heat map, where red represents increased expression and green decreased expression.

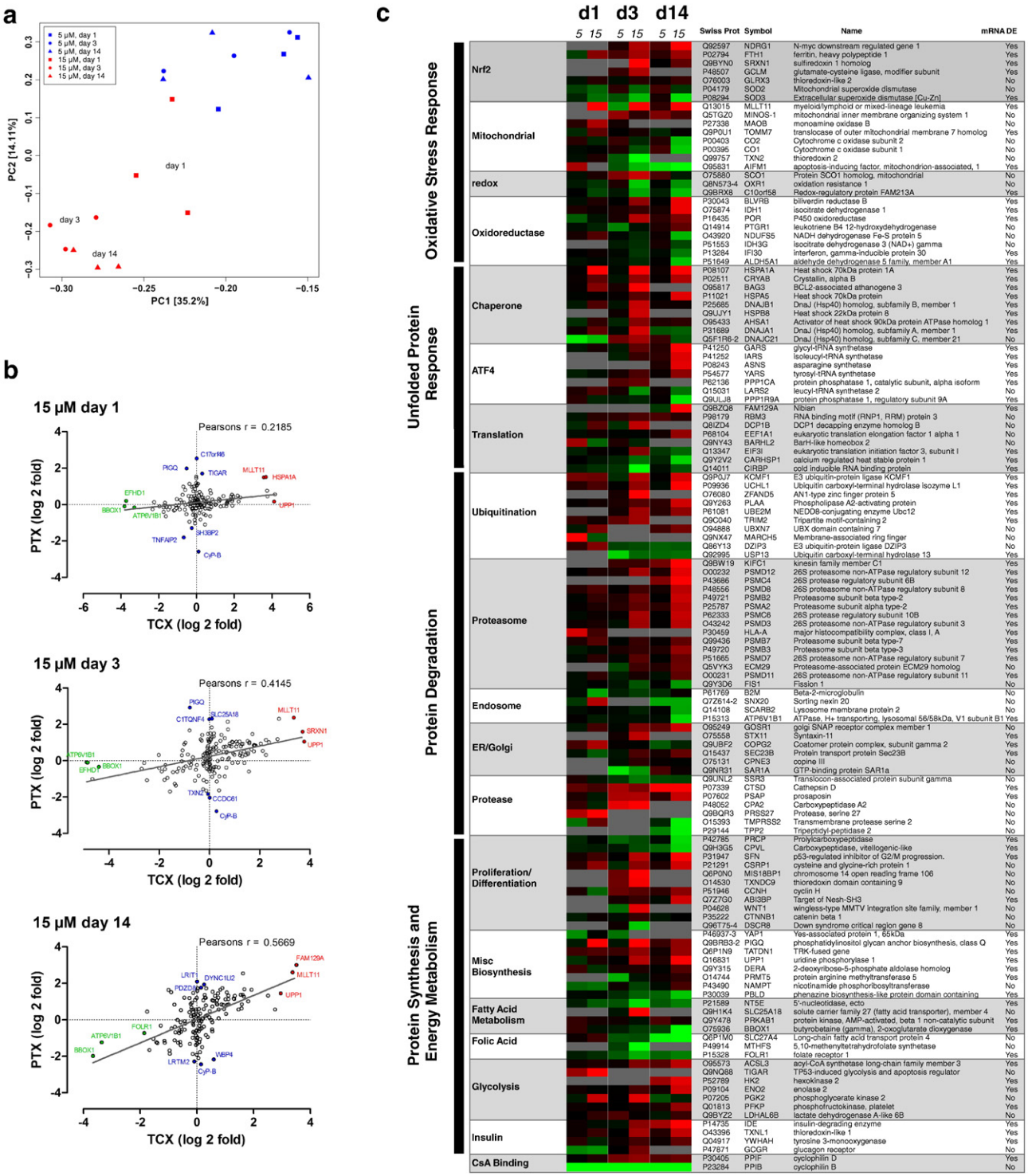

Fig. 3 – Effects of CsA exposure on RPTEC/TERT1 proteome. (a) PCA of all 599 proteins detected in every sample. (b) Correlation of CsA-induced protein alterations with corresponding mRNA levels. Red and green dots represent a good correlation of increased or decreased molecules, respectively. Blue dots show a poor correlation between mRNA and protein. (c) Heat map and functional grouping of proteins, with green indicating a decrease and red indicating an increase in protein abundance over control values. The mRNA DE (differentially expressed) column reports whether the corresponding mRNA was significantly deregulated.

transcript level. For example, *PIGQ* and *TIGAR* were marginally altered at the mRNA level but increased at the protein level (Fig. 3b), whereas PPP1CA was increased at the protein level but exhibited a decreased transcript level. Additionally, the fatty acid transporter SLC25A18, and CyP-B (aka PPIB) were only altered at the protein level. Examples of good correlations

between mRNA and protein levels include the decreased molecules butyrobetaine (gamma), 2-oxoglutarate dioxygenase (BBOX1) and ATPase, ATP6V1B1 and the increased molecules MLLT11 and HSPA1A, and SRXN1.

Functional evaluation of the proteins altered by 15 μM CsA demonstrated a dominance of oxidative stress response, mitochondrial dysfunction and protein degradation, which overlaps with the TCX data (Fig. 3c). In the ATF4 pathway, PPP1CA, ASNS, GARS, IARS and YARS were all induced. Additionally, there were alterations in chaperone proteins and proteins involved in translation. For the Nrf2 pathway, proteins including FTH1, SRXN1, GCLM and GLRX3 were elevated at one or more time points. Additionally, proteins known to be attenuated by Nrf2 activation were decreased, for example SOD3 [22]. A number of proteins not directly linked to Nrf2 but known to be altered by oxidative stress were also impacted here including, biliverdin reductase B (BLVRB) and oxidation resistance 1 (OXR1). Proteins associated with the mitochondria were also altered, including a decrease in cytochrome C oxidase (1 and 2) and an increase in MINOS-1 and MLLT11 (aka Af1q). The latter protein is thought to be involved in the regulation of mitochondrial membrane potential [23]. Proteins that are associated with ubiquitination, proteasome activation (PSMs) and lysosomal activity (including cathepsin D, CTSD) were induced (Fig. 3c). Proteins involved in protein synthesis and energy metabolism were also altered. Fatty acid metabolism was suppressed, for example, BBOX1 and the long chain fatty acid transporter SLC27A4 were decreased. Proteins involved in glycolysis were increased including, ENO2, HK2 and phosphofructokinase P (PFKP).

CyP-D was increased at days 3 and 14 (Fig. 3c). Interestingly, CyP-B was the only protein consistently attenuated by both CsA concentrations at all time points.

3.3. *MTX alterations*

3.3.1. *Extracellular*

PCA demonstrated a high impact of 15 μM CsA and a negligible effect of 5 μM on the metabolic profile in supernatant medium (Fig. 4a). The 15 μM samples demonstrated a time-dependent clustering pattern. There were 192 significant features with over 2 fold alteration at any day (Fig. 4b). At the present time deeper biological insights of the MTX supernatant data cannot be provided as the data set remains un-annotated.

3.3.2. *Cellular*

CsA (15 μM) had a considerable impact on cellular metabolites. Gamma-glutamylcysteine (γ-GC) was the most increased metabolite with an 80-fold induction at day 3 (Fig. 4c). Glutathione (GSH), glutathione disulfide (GSSG) and cysteine glutathione disulfide (CYSSG) were also heavily induced, demonstrating an induction of glutathione synthesis, recycling and oxidation. The amino acids L-alanine, L-arginine, L-leucine, L-tryptophan, L-valine and L-isoleucine were increased, while L-aspartate, L-threonine and L-glutamate were decreased. Fumarate was decreased while citrate and NADH were elevated. The nucleoside monophosphate sugar cytidine monophosphate N-acetylneuraminic acid (CMP-NeuNAc) was increased. CMP-NeuNAc is involved in glycosylation, specifically sialic acid addition, and its induction was paralleled by an increase in the mRNA for cytidine monophosphate N-acetylneuraminic acid synthetase (CMAS). Sphingomyelin was decreased while phosphatidylcholine (o-14:0/16:0) was increased after 14-day exposure. Finally, the osmolytes betaine and glycerophosphocholine (GPC) were decreased.

3.4. *CsA pharmacokinetics in vitro*

CsA was applied daily, thus resetting the concentration to 5 or 15 μM externally every 24 h. The measured CsA concentrations in the supernatant and cell lysates were superimposed with the best maximum posterior fit of the 3-compartment pharmacokinetic model (Fig. 5a). These predictions were generated from random, but plausible, parameter values. Overall the data is well simulated. The various curves reflect uncertainty in the model predictions, resulting from unavoidable measurement errors and modeling approximations. The posterior parameter distributions obtained after Markov-chain Monte Carlo sampling are summarized in Supplementary Table 1. CsA applied at 5 μM, demonstrated minor biokinetic alterations between day 0 and day 13 (Fig. 5b and c). Some adsorption to the plastic occurred rapidly, accounting for 6.9% of the corresponding quantity in the supernatant within 30 min and reaching its peak of 12% at 24 h on day 0. The unchanged values measured at day 13 indicate the saturation of the process. A steady-state regime was quickly reached with approximately 67% of CsA in the supernatant, 21% in the cells and 12% on the vial walls. The recovery of CsA was approximately 85% at each time point, indicating that CsA metabolism is limited.

CsA applied at 15 μM, showed major kinetic alterations over the time course (Fig. 5b and c), reflected in the increased uptake half time of 0.38 h on day 0 to 2.9 h on day 13. In addition there was an extremely high intracellular concentration at day 13, while the kinetics in the supernatant remained similar at both days. Approximate steady-state was reached in cells only after about 7 days and the distribution between supernatant, cells and vial walls was 48, 43, and 9%, respectively. The intracellular concentration measured at day 13 was 9.3 fold higher than that for 5 μM CsA. These values represent an abrupt non-linear accumulation of CsA in cells, with increasing concentrations and could not have been detected by a single administration. CsA recovery was approximately 85% at each time point. Plastic binding of 15 μM CsA took longer to saturate than 5 μM, also peaking at 12% (data not shown).

The global metabolomic alterations from Fig. 4b were superimposed on the cellular kinetic data and follow the time course of intra-cellular CsA concentrations closely (Fig. 5c, boxes).

3.5. *Cyclophilin B secretion*

While PTX analysis revealed that cellular CyP-B was reduced with both concentrations at all time points (Fig. 3b and c), there was no alteration in the mRNA level under any condition (Fig. 3b). Thus, it is likely that CsA is binding CyP-B resulting in secretion, as previously demonstrated [24]. Therefore, we investigated CyP-B content in cell lysates and supernatants. CsA induced a time-dependent increase in

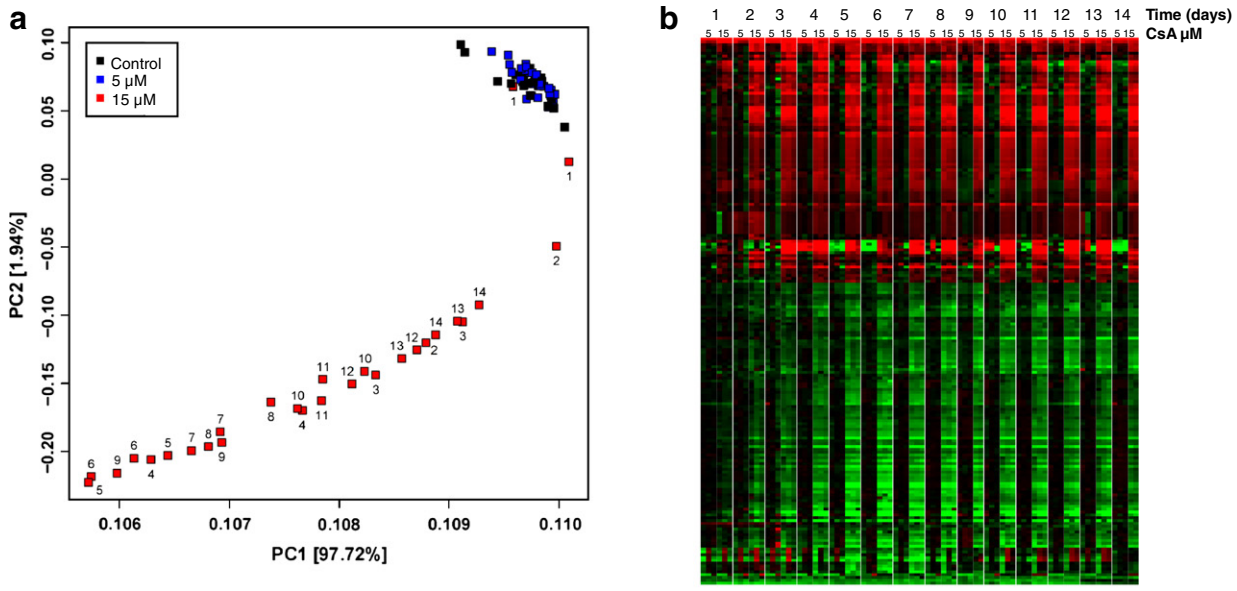

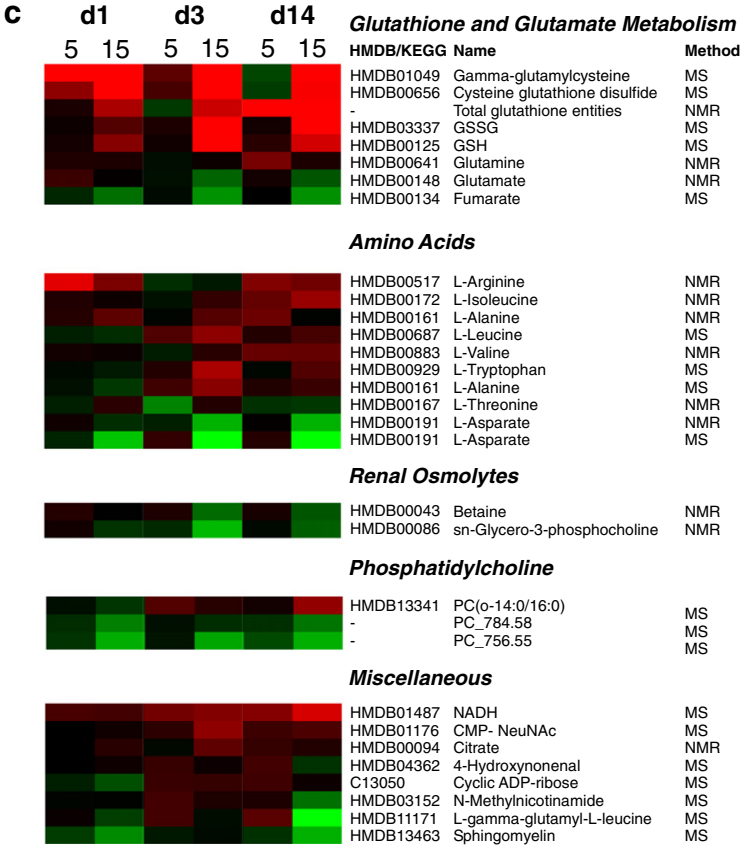

Fig. 4 – Effects of CsA exposure on RPTEC/TERT1 metabolome. (a) PCA of all measured metabolites. Numbers refer to exposure time. (b) Heat map of 192 features with significant (2 fold and p-value 0.001 cutoffs) alterations compared with time matched control. Each square represents a biological replicate (2 or 3) and colors are representative of log 2 fold time matched control values, where red is increased and green decreased. Metabolites are clustered using complete linkage. (c) Metabolites measured in cell extracts by ^{1}H NMR or MS as indicated. Values represent the mean log 2 fold control value from 3 biological replicates. Colors indicate increased (red) or decreased (green) metabolites. Abbreviations: CMP-NeuNAc Cytidine monophosphate N-acetylneuraminic acid.

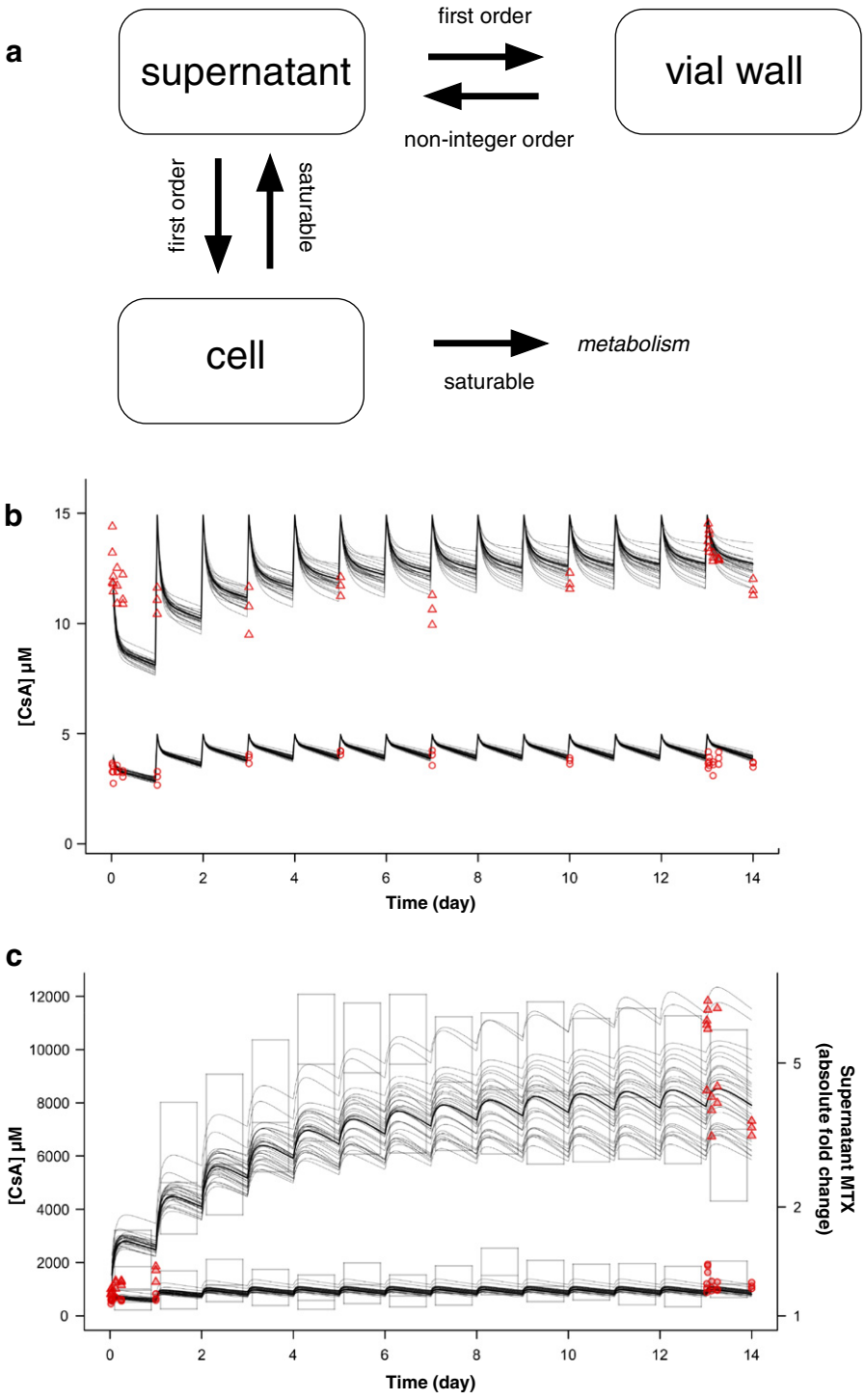

Fig. 5 – Pharmacokinetic modeling of CsA concentrations. (a) Diagram of the 3-compartment model of CsA pharmacokinetics. CsA concentration in supernatants (b) and cell lysate (c). The data values are given by either red circles (5 µM) or triangles (15 µM). Metabolomic data (absolute fold-change) are summarized by box plots (bottom middle and top lines are the first median and third quartile, respectively). Thick black lines are best-fit (maximum posterior probability) model predictions. Thin black lines are predictions using 30 different parameter sets.

CyP-B secretion with a concomitant decrease in cytosolic CyP-B (Fig. 6a). The time course and magnitude of these observations were almost identical for both concentrations. At 24 h exposure, secretion was maximal and very little CyP-B was observed in supernatants on subsequent exposure days (not shown). A dose–response relationship demonstrated a maximum secretion with 5.8 µM CsA at 24 h (Fig. 6b and c).

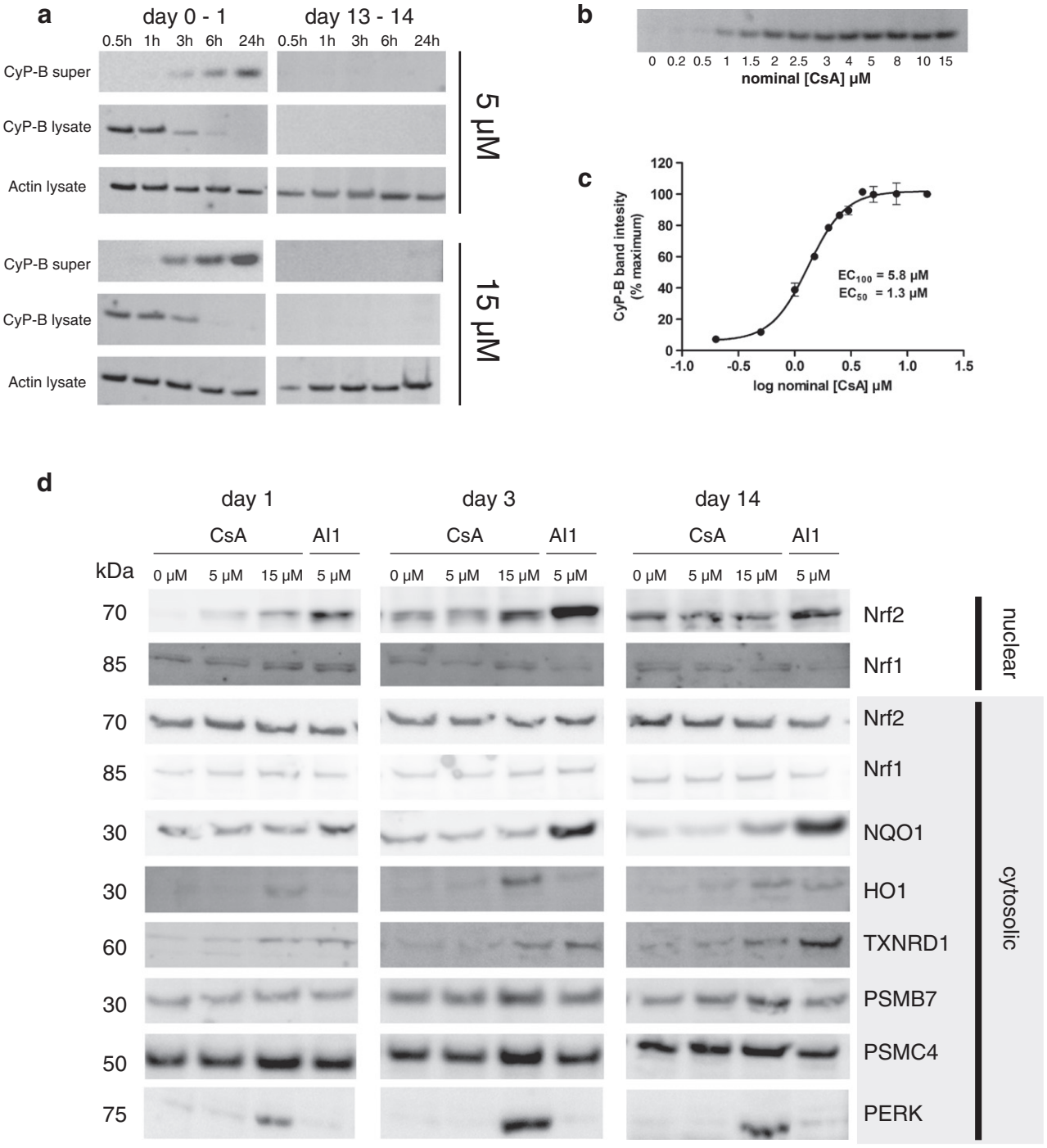

Fig. 6 – Effects of CsA on selected proteins by Western blot analysis. (a) CyP-B levels were detected in apical supernatant and cell lysates. The CyP-B band corresponds to 25.5 kDa. (b) RPTEC/TERT1 cultured and stabilized in 96 well plates were treated with CsA for 24 h. CyP-B was detected in the supernatant and (c) quantified by densitometry. (d) RPTEC/TERT1 cells cultured on 12 well plates were treated with CsA and the Nrf2 inducer, AI1 for 1, 3 and 14 days. Nuclear and cytosolic lysates were prepared.

3.6. *Effects of CsA and Nrf2 induction on selected proteins by Western blot analysis*

Since the Nrf2 oxidative stress response and the 26S proteasome pathways were both significantly altered, the two transcription factors Nrf2 and Nrf1, as well as some of their regulated proteins were investigated in more detail. In addition, as a representative protein of the UPR, PERK was also investigated further. Levels of Nrf2 increased in the nuclear fraction in response to 15 µM CsA and to the Nrf2 inducer AI1 (Fig. 6d). The response peaked at day 3 and returned to basal levels by day 14 for CsA but remained elevated for AI1. HO1 was increased in response to 15 µM CsA in

all time points, but only at day 14 for AI1 (Fig. 6d). Conversely, NQO1 was increased by AI1 at all time points but only at day 14 with CsA (Fig. 6d). TXNRD1 levels were increased in response to 15 μM CsA and AI1 at all time points. While we found no evidence for a CsA-induced increase in Nrf1 protein levels or nuclear translocation, two proteasome proteins of the 26S proteasome, PSMB7 (beta subunit of the 20S catalytic core) and PSMC4 (ATPase of the 19S regulatory unit) were increased by 15 μM CsA at all time points. In addition, 5 μM CsA increased PSMC4 levels slightly at day 14. AI1 on the other hand had no effect on PSMB7 or PSMC4 expression. PERK was induced with 15 μM CsA at all time points, with highest levels observed at day 3 (Fig. 6d). AI1 did not induce PERK levels indicating an Nfr2 independent effect.

4. Discussion

Integrating omic approaches is becoming more important in cellular and molecular biology and will most likely change the way we approach biological investigations [4]. However, attempts thus far to combine omic data streams have been met with limited success [2,25]. In the present study, we have brought together experts from the various fields of TCX, PTX, MTX, epithelial cell culture and pharmacokinetic modeling. The major aim was to investigate the benefit of integrating omic data streams and pharmacokinetics for application in drug safety, utilizing an *in vitro* system treated with CsA in repeat dose.

The discovery of the potent immunosuppressive properties of CsA revolutionized transplant medicine. Three decades later, CsA is still one of the leading immunosuppressive agents in clinical use. However, it was recognized early on that CsA is nephrotoxic, causing disturbances to the vasculature, the glomerulus and the proximal tubule [26–28]. In addition, CsA can also induce hepatotoxicity and cardiotoxicity [29]. Although it is a very well studied compound, its exact mechanism of toxicity is still not settled. Evidence from both *in vitro* and *in vivo* studies has implicated CsA-induced reactive oxygen species (ROS) as a potential toxicity mechanism and co-administration of antioxidants appears to ameliorate nephrotoxic outcome [29,30]. It is plausible that ROS is mitochondria-derived, especially since CsA has been shown to cause injury to isolated mitochondria and to mitochondria both *in vitro* and *in vivo* [27,31–34]. Indeed, CsA has been shown to interfere with the putative mitochondrial transition pore [35], to increase both inner mitochondrial membrane potential [36] and mitochondrial calcium loading [37]. Some of these events are thought to be mediated *via* CsA binding and modification of the mitochondrial protein CyP-D [38]. Thus, primary mitochondrial injury is an attractive theory for the harmful effects of CsA and may explain why cells with high mitochondrial volume fraction, such as proximal tubular cells, hepatocytes and cardiac myocytes are targets. Here, 15 μM CsA increased *CyP-D* mRNA and the protein was induced at both CsA concentrations. In addition, 15 μM CsA exposure resulted in an early induction of lactate production, a reduction in cellular fumarate, and an increase in cellular citrate and NADH. All of these metabolic alterations point to an inhibition of mitochondrial oxidative phosphorylation.

Mitochondrial injury can lead to oxidative stress and indeed the Nrf2-oxidative-stress pathway was enriched in all omic data sets with 15 μM CsA. We observed a robust increase in Nrf2 nuclear translocation and downstream targets, including *TXN*, *TXNRD1*, *HO1*, *NQO1* and *SRXN1*. A major effect of the Nrf2 defense mechanism is to increase glutathione reserves and enhance GSSG recycling to GSH, thereby redressing the highly oxidative environment. There was an obvious impact of CsA (15 μM) on the glutathione pathway, with an enhanced level of genes and proteins involved in glutathione synthesis and recycling (including *GCLM*, *GCLC* and *GSR*) increasing the cellular metabolites γ-GC and GSH.

It has also been suggested that CsA-induced proximal tubular toxicity is a result of ER stress and that ROS generation is a secondary event [39]. This is supported by a recent study which shows that antioxidant treatment does not prevent CsA-induced ER stress in HEK cells [11]. The unfolded protein response (UPR) is mounted when ER stress is detected and serves primarily to return normal ER function [40]. All three branches of the UPR were induced by 15 μM CsA and there was a strong signature of ATF4 activation in all omic data streams. Activation of PERK results in phosphorylation of the alpha domain of eukaryotic initiation factor 2 (eIF2), inhibiting its ability to initiate translation, thereby decreasing the load of nascent proteins entering the ER [41]. However, due to the presence of two upstream open reading frames (uORFs) in the 5′ leader of ATF4 mRNA, PERK activation actually increases the translation of ATF4 [42]. ATF4 is one of the main effectors of the UPR and promotes the transcription of genes involved in amino acid synthesis, amino acid transport and aminoacyl-tRNA synthesis [43]. Protein phosphatase 1 induction is a key negative feedback mechanism and acts to reactivate translation, by dephosphorylating eIF2α [44]. The regulatory subunit of protein phosphatase 1 (*PPP1R15A*) was increased in the TCX data and the catalytic subunit PPP1CA was increased in the PTX data. In addition, many of the aminoacyl-tRNA synthesis genes and proteins were induced. Asparagine synthetase (ASNS) was heavily induced in both TCX and PTX data sets. ASNS catalyzes the glutamine- and ATP-dependent conversion of aspartic acid to asparagine [43], producing in the process glutamate, a precursor for glutathione synthesis. Both glutamate and glutathione metabolic pathways were severely affected. A number of amino acid transporters and intracellular amino acids were induced here. Interestingly, Nrf2 increases ATF4 transcription [21] and thus acts as a primer for UPR. ATF4 mRNA was heavily induced at all time points.

There was a strong induction of the PSM, proteasomal family members at both the mRNA and protein levels at all three time points by 15 μM CsA. Such a rigorous induction of protein ubiquitination and proteasomal degradation is likely to necessitate removal of oxidized proteins and would be expected to run in parallel to Nrf2 activation. There has even been a suggestion that Nrf2 may directly regulate proteasomal activity [45]. However, under our experimental conditions this was not the case, as the Nrf2 activator AI1 efficiently activated Nrf2 without increasing the two proteasomal proteins PSMB7 and PSMC4. Recent evidence has shown that the proteasome is likely under the transcriptional control of the related transcription factor, Nrf1 [46]. Nrf1 was up-regulated here at the transcript level

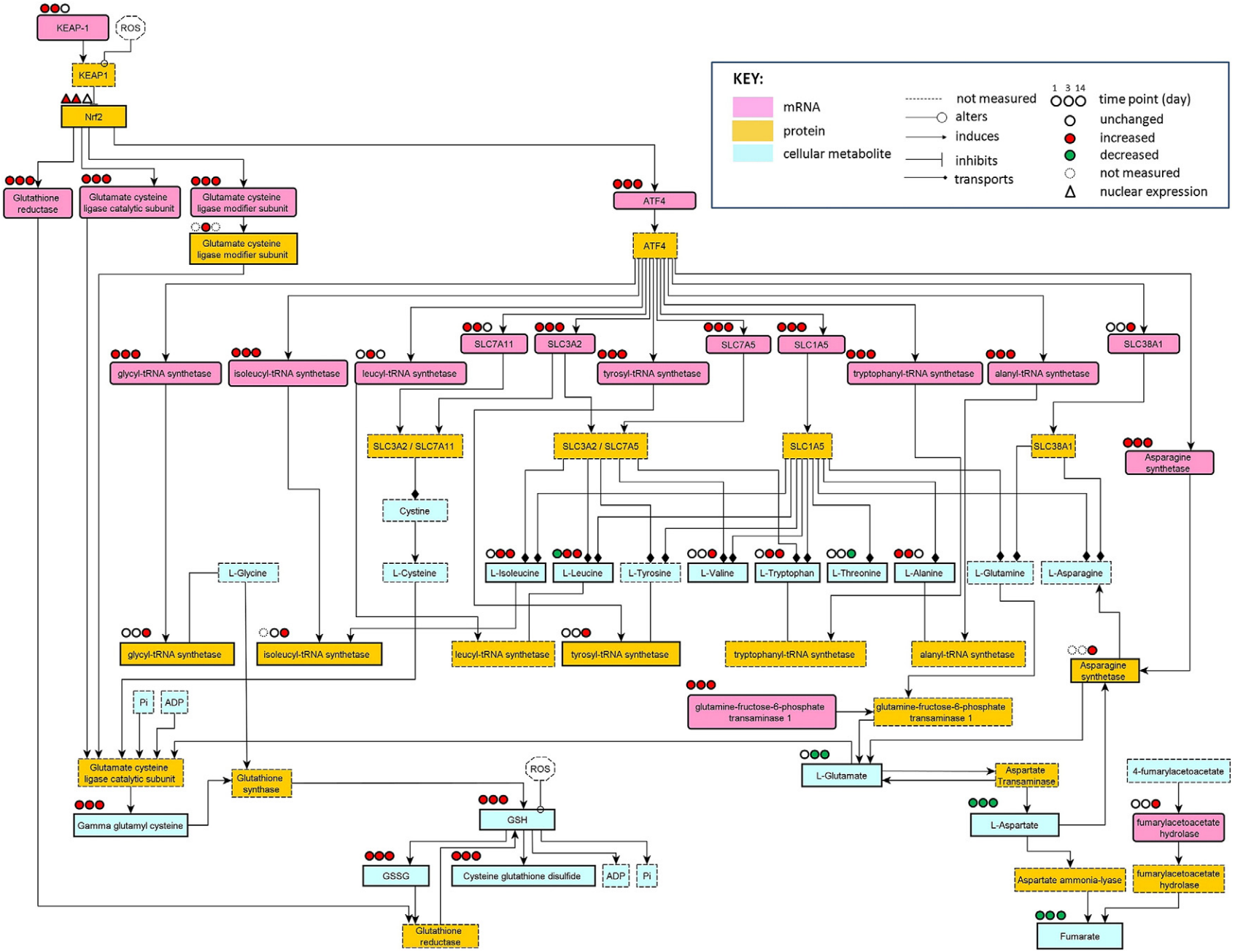

Fig. 7 – Integration of CsA induced mRNA, protein and metabolites from omic data. Starting from the cellular MTX analysis the pathway was expanded from the available PTX and TCX data. The data shows Nrf2 and ATF4 as major hubs and the interaction between them. The program YEd from the software developers YWorks was used to organize the data.

at all time points. However, there were no alterations in Nrf1 cytosolic or nuclear protein levels. Thus it remains unclear if Nrf1 is directly involved in the proteasomal response observed here.

Cyclophilins are the primary molecular target of CsA [47] and the complex of CsA and cyclophilin leads to calcineurin inhibition and is responsible for the immunosuppressive effects [48]. Cyclophilins have a peptidyl-prolyl *cis–trans* isomerase (PPIase) activity and function as molecular chaperones. While all cyclophilin family members bind CsA, only CsA/CyP-A and CsA/CyP-B have been shown to inhibit calcineurin activity [49,50]. In the current study, CyP-B was the most decreased cellular protein identified by PTX at both CsA concentrations at all time points, while being unaffected at the mRNA level. Thus, we speculated that CsA exposure may induce CyP-B secretion as has been previously demonstrated in other cell culture models [24,51]. Western blot analysis confirmed that CsA induced CyP-B secretion. Interestingly, CyP-B was found only in the apical compartment, suggesting polarized secretion. It has been suggested that calcineurin inhibition is directly involved in the side effects of CsA [52,53]. However, our results provide compelling evidence for a calcineurin independent toxicity mechanism, as both 5 and 15 μM resulted in complete loss of cytosolic CyP-B, but no cell stress was observed at 5 μM over 14 days exposure.

The applicability of sensitive high-content omic technologies and the extraction of meaningful data are highly dependent on the use of well defined, standardized, stable and relevant biological systems. The *in vitro* model we have employed is first stabilized for 10 days at confluence, allowing complete contact inhibition. We have shown that under these conditions there is no longer a time-dependent alteration in the transcriptome of untreated cells. This is likely a key factor to the success of the omic comparisons carried out in this cell model.

An obvious, yet often overlooked, aspect of *in vitro* approaches to drug safety assessment is the bioavailability of the compound and the concentration of the parent compound within cells as a function of time. Without this information it is not possible to compare with corresponding *in vivo* data. Here we used LC–MS/MS to quantify the distribution of CsA over time and constructed a pharmacokinetic model. The model describes a rapid cellular uptake and accumulation of CsA, which is to be expected for a highly lipophilic compound. Application of 5 μM CsA resulted in an intracellular steady-state after 2 days of ~860 μM, while 15 μM reached a steady-state after 7 days, at an intracellular concentration of ~7600 μM. Thus, there is a non-linear dose–response relationship of external to internal CsA concentration due to bioaccumulation of CsA. This may be related to saturation of the p-glycoprotein extrusion pump at concentrations above 5 μM. The peak concentration of CsA in human blood, at therapeutic concentrations, has been reported to be between 100 and 830 nM [54,55]. However, it is well established that due to the lipophilicity of CsA, such measurements are highly dependent on factors including BMI, the level of lipoproteins and hematocrit level. A post-mortem study calculated that CsA is 53 times higher, on a per weight basis, in various tissues than accompanying blood samples [56]. Since we have employed a serum and blood free system, the higher accumulation of 215 fold for 5 μM CsA is to be expected (calculated from the average of day 13 measurements). Tissue-specific toxicities are often due to accumulation in the target tissue such as the kidney and thus this information is critical for safety evaluation. Assessment based on nominal concentrations *in vitro* or plasma levels *in vivo* alone, is imprecise, as tissue concentrations could be, as shown here for the high concentration of CsA, far above a safe threshold.

In summary, the results clearly show that cells are simultaneously experiencing mitochondrial perturbations, oxidative- and ER-stress only at the high CsA concentration. However, CyP-B secretion was maximum already at the low CsA concentration. This study demonstrates that *in vitro* cell culture systems coupled with pharmacokinetics and high content omic approaches can give extremely detailed and quantitative insights into both the pharmacological and toxicological effects of compounds. We also demonstrate the added value of integrating these techniques as illustrated in Fig. 7. In addition, the PTX data did not merely mirror the TCX data, but provided further information on key events, such as CyP-B secretion that is independent from gene transcription. MTX data provided an additional level of information and was particularly useful for assessing mitochondrial perturbations, a common target of xenobiotics. In conclusion, an integrated omic approach combined with stable human-derived *in vitro* cell culture models has the potential to considerably advance our understanding of chemical induced cellular perturbations and will be an extremely useful approach to drug safety paradigms.

Supplementary data to this article can be found online at http://dx.doi.org/10.1016/j.jprot.2012.11.022.

Acknowledgments

This project was funded by the European Union's 7th Framework Programme (FP7/2007–2013) under grant agreement no 202222, Predict-IV. The administrative and organization skills of Hannelore Popa-Henning are also much appreciated.

REFERENCES

[1] Wieser M, Stadler G, Jennings P, Streubel B, Pfaller W, Ambros P, et al. hTERT alone immortalizes epithelial cells of renal proximal tubules without changing their functional characteristics. Am J Physiol Renal Physiol 2008;295: F1365–75.
[2] Cramer GR, Urano K, Delrot S, Pezzotti M, Shinozaki K. Effects of abiotic stress on plants: a systems biology perspective. BMC Plant Biol 2011;11:163.
[3] He JC, Chuang PY, Ma'ayan A, Iyengar R. Systems biology of kidney diseases. Kidney Int 2012;81:22–39.
[4] Tan KC, Ipcho SV, Trengove RD, Oliver RP, Solomon PS. Assessing the impact of transcriptomics, proteomics and metabolomics on fungal phytopathology. Mol Plant Pathol 2009;10:703–15.

[5] Zhang SZ, Ye ZG, Xia Q, Zhang W, Bruce I. Inhibition of mitochondrial permeability transition pore: a possible mechanism for cardioprotection conferred by pretreatment with tanshinone IIA. Conf Proc IEEE Eng Med Biol Soc 2005;3: 2276–9.
[6] Wilmes A, Crean D, Aydin S, Pfaller W, Jennings P, Leonard MO. Identification and dissection of the Nrf2 mediated oxidative stress pathway in human renal proximal tubule toxicity. Toxicol In Vitro 2011;25:613–22.
[7] Jennings P, Aydin S, Bennett J, McBride R, Weiland C, Tuite N, et al. Inter-laboratory comparison of human renal proximal tubule (HK-2) transcriptome alterations due to cyclosporine A exposure and medium exhaustion. Toxicol In Vitro 2009;23: 486–99.
[8] Zidek N, Hellmann J, Kramer PJ, Hewitt PG. Acute hepatotoxicity: a predictive model based on focused illumina microarrays. Toxicol Sci 2007;99:289–302.
[9] Jennings P, Limonciel A, Felice L, Leonard MO. An overview of transcriptional regulation in response to toxicological insult. Arch Toxicol 2013;87(1):49–72.
[10] Ellis JK, Athersuch TJ, Cavill R, Radford R, Slattery C, Jennings P, et al. Metabolic response to low-level toxicant exposure in a novel renal tubule epithelial cell system. Mol Biosyst 2011;7: 247–57.
[11] Lamoureux F, Mestre E, Essig M, Sauvage FL, Marquet P, Gastinel LN. Quantitative proteomic analysis of cyclosporine-induced toxicity in a human kidney cell line and comparison with tacrolimus. J Proteomics 2011;75:677–94.
[12] Ellinger-Ziegelbauer H, Adler M, Amberg A, Brandenburg A, Callanan JJ, Connor S, et al. The enhanced value of combining conventional and "omics" analyses in early assessment of drug-induced hepatobiliary injury. Toxicol Appl Pharmacol 2011;252:97–111.
[13] Adler S, Basketter D, Creton S, Pelkonen O, van Benthem J, Zuang V, et al. Alternative (non-animal) methods for cosmetics testing: current status and future prospects—2010. Arch Toxicol 2011;85:367–485.
[14] Limonciel A, Aschauer L, Wilmes A, Prajczer S, Leonard MO, Pfaller W, et al. Lactate is an ideal non-invasive marker for evaluating temporal alterations in cell stress and toxicity in repeat dose testing regimes. Toxicol In Vitro 2011;25:1855–62.
[15] Sturm M, Bertsch A, Gropl C, Hildebrandt A, Hussong R, Lange E, et al. OpenMS — an open-source software framework for mass spectrometry. BMC Bioinformatics 2008;9:163.
[16] Junker J, Bielow C, Bertsch A, Sturm M, Reinert K, Kohlbacher O. TOPPAS: a graphical workflow editor for the analysis of high-throughput proteomics data. J Proteome Res 2012;11(7): 3914–20.
[17] Breitwieser FP, Muller A, Dayon L, Kocher T, Hainard A, Pichler P, et al. General statistical modeling of data from protein relative expression isobaric tags. J Proteome Res 2011;10:2758–66.
[18] Simon R, Lam A, Li MC, Ngan M, Menenzes S, Zhao Y. Analysis of gene expression data using BRB-ArrayTools. Cancer Inform 2007;3:11–7.
[19] Duff T, Carter S, Feldman G, McEwan G, Pfaller W, Rhodes P, et al. Transepithelial resistance and inulin permeability as endpoints in in vitro nephrotoxicity testing. Altern Lab Anim 2002;30(Suppl. 2):53–9.
[20] Martin-Martin N, Dan Q, Amoozadeh Y, Waheed F, McMorrow T, Ryan MP, et al. RhoA and Rho kinase mediate cyclosporine A and sirolimus-induced barrier tightening in renal proximal tubular cells. Int J Biochem Cell Biol 2012;44:178–88.
[21] Miyamoto N, Izumi H, Miyamoto R, Bin H, Kondo H, Tawara A, et al. Transcriptional regulation of activating transcription factor 4 under oxidative stress in retinal pigment epithelial ARPE-19/HPV-16 cells. Invest Ophthalmol Vis Sci 2011;52: 1226–34.
[22] Reddy NM, Kleeberger SR, Yamamoto M, Kensler TW, Scollick C, Biswal S, et al. Genetic dissection of the Nrf2-dependent redox signaling-regulated transcriptional programs of cell proliferation and cytoprotection. Physiol Genomics 2007;32: 74–81.
[23] Co NN, Tsang WP, Wong TW, Cheung HH, Tsang TY, Kong SK, et al. Oncogene AF1q enhances doxorubicin-induced apoptosis through BAD-mediated mitochondrial apoptotic pathway. Mol Cancer Ther 2008;7:3160–8.
[24] Price ER, Jin M, Lim D, Pati S, Walsh CT, McKeon FD. Cyclophilin B trafficking through the secretory pathway is altered by binding of cyclosporin A. Proc Natl Acad Sci U S A 1994;91:3931–5.
[25] Zhang W, Li F, Nie L. Integrating multiple 'omics' analysis for microbial biology: application and methodologies. Microbiology 2010;156:287–301.
[26] Burdmann EA, Yu L, Andoh TF, Perico C, Bennett WM. Calcineurin inhibitors and sirolimus. Clinical nephrotoxins: renal injury from drugs and chemicals2nd edition. ; 2003. p. 403–58.
[27] Pfaller W, Kotanko P, Bazzanella A. Morphological and biochemical observations in rat nephron epithelia following cyclosporine A (CsA) treatment. Clin Nephrol 1986;25(Suppl. 1):S105–10.
[28] Olbricht CJ, Steinker M, Auch-Schwelk W, Bossaller C, Haas J, Koch KM. Effect of cyclosporin on kidney proteolytic enzymes in men and rats. Nephrol Dial Transplant 1994;9:22–6.
[29] Rezzani R. Exploring cyclosporine A-side effects and the protective role-played by antioxidants: the morphological and immunohistochemical studies. Histol Histopathol 2006;21:301–16.
[30] Jennings P, Koppelstaetter C, Aydin S, Abberger T, Wolf AM, Mayer G, et al. Cyclosporine A induces senescence in renal tubular epithelial cells. Am J Physiol Renal Physiol 2007;293: F831–8.
[31] Hay R, Tammi K, Ryffel B, Mihatsch MJ. Alterations in molecular structure of renal mitochondria associated with cyclosporine A treatment. Clin Nephrol 1986;25(Suppl. 1):S23–6.
[32] Henke W, Nickel E, Jung K. Cyclosporine A inhibits ATP net uptake of rat kidney mitochondria. Biochem Pharmacol 1992;43:1021–4.
[33] Jung K, Reinholdt C, Scholz D. Inhibitory effect of cyclosporine on the respiratory efficiency of isolated human kidney mitochondria. Transplantation 1987;43:162–3.
[34] Strzelecki T, Khauli RB, Kumar S, Menon M. In vitro effects of cyclosporine on function of rat kidney mitochondria. Transplant Proc 1987;19:1393–4.
[35] Bernardi P, Broekemeier KM, Pfeiffer DR. Recent progress on regulation of the mitochondrial permeability transition pore; a cyclosporin-sensitive pore in the inner mitochondrial membrane. J Bioenerg Biomembr 1994;26:509–17.
[36] Bernardi P. The permeability transition pore control points of a cyclosporin A-sensitive mitochondrial channel involved in cell death. Biochim Biophys Acta 1996;1275:5–9.
[37] Wei AC, Liu T, Cortassa S, Winslow RL, O'Rourke B. Mitochondrial Ca^{2+} influx and efflux rates in guinea pig cardiac mitochondria: low and high affinity effects of cyclosporine A. Biochim Biophys Acta 2011;1813:1373–81.
[38] Azzolin L, von Stockum S, Basso E, Petronilli V, Forte MA, Bernardi P. The mitochondrial permeability transition from yeast to mammals. FEBS Lett 2010;584:2504–9.
[39] Sarro E, Jacobs-Cacha C, Itarte E, Meseguer A. A pharmacologically-based array to identify targets of cyclosporine A-induced toxicity in cultured renal proximal tubule cells. Toxicol Appl Pharmacol 2012;258:275–87.
[40] Lin JH, Lavail MM. Misfolded proteins and retinal dystrophies. Adv Exp Med Biol 2010;664:115–21.
[41] Walter P, Ron D. The unfolded protein response: from stress pathway to homeostatic regulation. Science 2011;334:1081–6.

[42] Vattem KM, Wek RC. Reinitiation involving upstream ORFs regulates ATF4 mRNA translation in mammalian cells. Proc Natl Acad Sci U S A 2004;101:11269–74.
[43] Siu F, Bain PJ, LeBlanc-Chaffin R, Chen H, Kilberg MS. ATF4 is a mediator of the nutrient-sensing response pathway that activates the human asparagine synthetase gene. J Biol Chem 2002;277:24120–7.
[44] Ma Y, Hendershot LM. Delineation of a negative feedback regulatory loop that controls protein translation during endoplasmic reticulum stress. J Biol Chem 2003;278:34864–73.
[45] Pickering AM, Linder RA, Zhang H, Forman HJ, Davies KJ. Nrf2-dependent induction of proteasome and Pa28alphabeta regulator are required for adaptation to oxidative stress. J Biol Chem 2012;287:10021–31.
[46] Steffen J, Seeger M, Koch A, Kruger E. Proteasomal degradation is transcriptionally controlled by TCF11 via an ERAD-dependent feedback loop. Mol Cell 2010;40:147–58.
[47] Harding MW, Handschumacher RE. Cyclophilin, a primary molecular target for cyclosporine. Structural and functional implications. Transplantation 1988;46:29S–35S.
[48] Walsh CT, Zydowsky LD, McKeon FD. Cyclosporin A, the cyclophilin class of peptidylprolyl isomerases, and blockade of T cell signal transduction. J Biol Chem 1992;267:13115–8.
[49] Swanson SK, Born T, Zydowsky LD, Cho H, Chang HY, Walsh CT, et al. Cyclosporin-mediated inhibition of bovine calcineurin by cyclophilins A and B. Proc Natl Acad Sci U S A 1992;89:3741–5.
[50] Bram RJ, Hung DT, Martin PK, Schreiber SL, Crabtree GR. Identification of the immunophilins capable of mediating inhibition of signal transduction by cyclosporin A and FK506: roles of calcineurin binding and cellular location. Mol Cell Biol 1993;13:4760–9.
[51] Fearon P, Lonsdale-Eccles AA, Ross OK, Todd C, Sinha A, Allain F, et al. Keratinocyte secretion of cyclophilin B via the constitutive pathway is regulated through its cyclosporin-binding site. J Invest Dermatol 2011;131: 1085–94.
[52] Grinyo JM, Cruzado JM. Cyclosporine nephrotoxicity. Transplant Proc 2004;36:240S–2S.
[53] Naesens M, Kuypers DR, Sarwal M. Calcineurin inhibitor nephrotoxicity. Clin J Am Soc Nephrol 2009;4:481–508.
[54] Fukudo M, Yano I, Masuda S, Fukatsu S, Katsura T, Ogura Y, et al. Pharmacodynamic analysis of tacrolimus and cyclosporine in living-donor liver transplant patients. Clin Pharmacol Ther 2005;78:168–81.
[55] Akhlaghi F, Keogh AM, McLachlan AJ, Kaan A. Pharmacokinetics of cyclosporine in heart transplant recipients receiving metabolic inhibitors. J Heart Lung Transplant 2001;20:431–8.
[56] Lensmeyer GL, Wiebe DA, Carlson IH, Subramanian R. Concentrations of cyclosporin A and its metabolites in human tissues postmortem. J Anal Toxicol 1991;15:110–5.